FABAD J. Pharm. Sci., 51, 3, 1315-1340, 2026
Doi: 10.55262/fabadeczacilik.1860907
RESEARCH ARTICLE

An Immunoinformatics-Based Multi-Epitope Vaccine Targeting Multiple Stages of Tuberculosis Pathogenesis

Sema KARABUDAK[*°], Sümeyye ALTUNOK[**], Emre Can BULUZ[***]

An Immunoinformatics-Based Multi-Epitope Vaccine Targeting Multiple Stages of Tuberculosis Pathogenesis

SUMMARY

Tuberculosis (TB), caused by M. tuberculosis, remains one of the leading causes of mortality from infectious diseases worldwide, underscoring the urgent need for more effective vaccine strategies. Advances in immunoinformatics have enabled rational, cost-effective vaccine design through systematic epitope identification and optimization. In this study, a multi-epitope vaccine candidate was computationally designed by integrating cytotoxic T lymphocyte (CTL), helper T lymphocyte (HTL), and B-cell epitopes derived from three M. tuberculosis antigens associated with distinct stages of infection: Ag85B, ESAT-6, and HspX. Selected epitopes were screened for antigenicity, immunogenicity, allergenicity, toxicity, and global population coverage, and assembled into a single construct using rational linker and adjuvant strategies. Structural modeling and refinement were performed, followed by molecular docking and molecular dynamics simulations to evaluate interactions with human Toll-like receptors (TLRs), namely TLR2, TLR4, and TLR9. The designed construct was predicted to exhibit favorable antigenic and safety profiles, structural stability, and broad population coverage. Docking, molecular dynamics, and binding free energy analyses suggested the possibility of stable and energetically favorable interactions with all three TLRs, with comparatively stronger binding for the TLR9 complex. In silico immune simulations indicated the potential to induce cellular and humoral immune responses, accompanied by increased interferon-γ (IFN-γ) and interleukin-2 (IL-2) levels and a possible formation of immunological memory. Overall, this study proposes a stage-spanning multi-epitope TB vaccine candidate and outlines an immunoinformatics-based design framework that may support future experimental validation and optimization.

Keywords: *Reverse vaccinology, immunoinformatics, T-cell epitopes, B-cell epitopes, tuberculosis (TB).*

Tüberkülozun Farklı Evrelerini Hedefleyen, İmmünoinformatik Yöntemlerle Tasarlanmış Çoklu Epitop Aşı

ÖZ

Tüberküloz (TB), Mycobacterium tuberculosis (M. tuberculosis) tarafından oluşturulan ve dünya genelinde bulaşıcı hastalıklar arasında ölüme en sık yol açan hastalıklardan biri olmaya devam etmektedir. Bu durum, daha etkili aşı stratejilerine duyulan acil ihtiyacı ortaya koymaktadır. İmmünoinformatik alanındaki gelişmeler, epitopların sistematik olarak belirlenmesi ve optimize edilmesi yoluyla rasyonel ve maliyet-etkin aşı tasarımını mümkün kılmıştır. Bu çalışmada, enfeksiyonun farklı evreleriyle ilişkili üç M. tuberculosis antijeninden (Ag85B, ESAT-6 ve HspX) türetilen sitotoksik T lenfosit (CTL), yardımcı T lenfosit (HTL) ve B hücre epitoplarının entegrasyonu ile çok epitoplu bir aşı adayı hesaplamalı olarak tasarlanmıştır. Seçilen epitoplar; antijenisite, immünojenisite, alerjenite, toksisite ve küresel popülasyon kapsamı açısından taranmış ve rasyonel bağlayıcı (linker) ve adjuvan stratejileri kullanılarak tek bir yapı halinde birleştirilmiştir. Yapısal modelleme ve iyileştirme işlemlerinin ardından, insan Toll-benzeri reseptörleri (TLR) olan TLR2, TLR4 ve TLR9 ile olası etkileşimleri değerlendirmek amacıyla moleküler yerleştirme ve moleküler dinamik simülasyonları gerçekleştirilmiştir. Tasarlanan yapının, antijenik ve güvenlik özellikleri açısından uygun bir profile sahip olabileceği, yapısal stabilite gösterebileceği ve geniş popülasyon kapsamı sağlayabileceği öngörülmüştür. Moleküler yerleştirme, moleküler dinamik simulasyonlar ve bağlanma serbest enerjisi analizleri, her üç TLR ile de stabil ve enerjik olarak elverişli etkileşimlerin mümkün olabileceğini göstermiş olup TLR9 kompleksi için nispeten daha güçlü bir bağlanma öngörülmüştür. In silico bağışıklık simülasyonları, artmış interferon-γ (IFN-γ) ve interlökin-2 (IL-2) düzeyleri ile birlikte hücresel ve humoral bağışıklık yanıtlarının oluşma potansiyeline işaret etmiş ve immünolojik hafıza oluşabileceğini göstermiştir. Sonuç olarak bu çalışma, enfeksiyonun farklı evrelerini kapsayan çok epitoplu bir TB aşı adayını önermekte ve gelecekte yapılacak deneysel doğrulama ve optimizasyon çalışmalarını destekleyebilecek immünoinformatik temelli bir tasarım çerçevesi sunmaktadır.

Anahtar Kelimeler: *Ters aşılama, immünoinformatik, T-hücre epitopu, B-hücre epitopu, tüberküloz (TB).*

Recieved: 11.01.2026
Revised: 01.08.2026
Accepted: 25.09.2026

[*] ORCID: 0000-0002-3646-0442, Ankara Yıldırım Beyazıt University Faculty of Medicine, Department of Medical Genetics, Ankara, Türkiye; Ankara Yıldırım Beyazıt University Central Research Laboratory Application and Research Center, Ankara, Türkiye
[**] ORCID: 0000-0002-9004-0617, The Ohio State University Wexner Medical Center, Department of Neurology Columbus, 43210, OH, United States
[***] ORCID: 0000-0002-2491-4347, Ege University, Department of Physics, Institute of Science and Technology, 35100, Bornova, İzmir, Türkiye

[°] Corresponding Author; Sema Karabudak
E-mail: semakarabudak@aybu.edu.tr

INTRODUCTION

Tuberculosis (TB), caused by *M. tuberculosis*, is one of the most significant causes of death from infectious diseases worldwide. In 2023, TB surpassed COVID-19 as the leading cause of death from infectious diseases, with over twice as many deaths as HIV/AIDS (Suvvari, 2025). TB mortality reaches up to 50% without treatment (WHO, 2023a), and treatment success rates using the current WHO Recommended Drug Regimens remain limited at approximately 65-75% (WHO, 2025). Access to appropriate therapy continues to be hindered by socioeconomic and health-related factors such as poverty, malnutrition, HIV infection, tobacco use, and diabetes (Teibo et al., 2024), all of which further exacerbate the global TB burden.

Tuberculosis remains a major global health burden. According to the World Health Organization (WHO) Global Tuberculosis Report 2022, an estimated 10.6 million people developed tuberculosis in 2021, indicating that the global incidence of the disease continues to exceed 10 million cases annually despite international control efforts (WHO, 2022). This alarming trend highlights the inadequacy of current TB control strategies and emphasizes the urgent need for innovative preventive measures. In response, the United Nations (UN) and WHO have jointly launched an emergency action plan aimed at ending the global TB epidemic by 2030 (Stop TB Partnership, 2022). To strengthen international control efforts, the United Nations convened two high-level TB meetings in 2018 (United Nations General Assembly, 2018) and 2023 (WHO, 2023b), incorporating new strategic commitments into the existing global TB framework (United Nations General Assembly, 2023). Since 1997, WHO's annual TB reports have played a pivotal role in monitoring disease trends, guiding interventions, and refining policy objectives (WHO, 2020).

The Bacillus Calmette–Guérin (BCG) remains the only licensed TB vaccine and has been in use for nearly a century. Although BCG provides partial protection against severe TB in children, its efficacy against adult pulmonary TB is limited (Ari, Beig, Sholeh, & Khoshmirsafa, 2024). Moreover, its effectiveness varies across geographic regions; it is not considered safe for immunocompromised individuals, and it fails to induce durable immunity or prevent latent TB infection (WHO, 2024). These limitations underscore the critical need for next-generation vaccines capable of eliciting stronger, broader, and longer-lasting immune protection.

In recent years, *in silico* vaccine design has emerged as a powerful and cost-effective approach in the fight against infectious diseases (Ali et al., 2024; Bahadori et al., 2022; Jiang et al., 2023; Zubair et al., 2025). Computational immunology and bioinformatics tools enable the precise identification, evaluation, and integration of immunogenic epitopes into rationally designed constructs (Bulla, Sbano da Silva, Prado Sereno, Ribeiro Dias, & Leal da Silva, 2025). Notably, multi-epitope vaccines have garnered increasing attention for their ability to simultaneously stimulate both humoral and cell-mediated immune responses (Urdahl, 2014). Such vaccines can engage immune pathways through major histocompatibility complexes (MHC) and toll-like receptors (TLRs), thereby inducing CTL and HTL responses (Deepthi, Sasikumar, Mohanakumar, & Rajamma, 2025; Hashempour et al., 2024). Meanwhile, B-cell epitopes contribute to long-term protection by promoting the production of neutralizing antibodies (Lim et al., 2022). Careful selection of epitopes is thus essential to ensuring a potent and targeted immune response (Musunuri, Weidenbacher, & Kim, 2024). Compared to single-subunit vaccines, multi-epitope constructs provide broader and more comprehensive protection against the complex infection dynamics of TB (Akurut et al., 2025; Barazani, Erdos, Chowdhury, Kaur, & Venketaraman, 2025; Faysal et al., 2024; Yun et al., 2024).

In the context of tuberculosis vaccine design, antigen selection requires careful evaluation of immunogenic potential, functional roles at different stages

of infection, and complementary immune activation profiles. Antigen 85B (Ag85B), a key component of the antigen 85 complex, is predominantly associated with the active phase of infection and plays a central role in mycobacterial cell wall biosynthesis, making it a well-established immunodominant antigen capable of inducing both $CD4^+$ and $CD8^+$ T-cell responses (An et al., 2025). Early secretory antigenic target-6 (ESAT-6), a virulence factor secreted via the ESX-1 system, contributes to immune modulation and cytosolic escape of *M. tuberculosis* and elicits strong interferon-γ–mediated cellular immune responses during early infection (Anes, Pires, Mandal, & Azevedo-Pereira, 2023). In contrast, heat shock protein X (HspX), also known as α-crystallin, is primarily expressed during latent infection and plays a key role in bacterial persistence under hypoxic and stress conditions, and is therefore considered a hallmark antigen of latent tuberculosis infection (Lew, Norazmi, Nordin, & Tye, 2022). Collectively, these antigens may provide a rational basis for a vaccine strategy targeting complementary stages of the tuberculosis infection cycle.

Although several immunoinformatics-based studies have proposed multi-epitope vaccine designs against *Mycobacterium tuberculosis*, many rely on numerous antigens or focus on proteins expressed during a single stage of infection, which may increase construct complexity without ensuring balanced immune recognition across the pathogen life cycle. In this study, a stage-integrated antigen selection strategy was adopted by combining epitopes derived from ESAT-6, Ag85B, and HspX to generate a streamlined multi-epitope construct intended to capture key immunological features of both active and dormant infection. While similar antigen combinations have been explored previously, most studies have focused primarily on epitope prediction and static docking analyses involving a single innate immune receptor. In contrast, the present study evaluates the proposed construct using a multi-layered immunoinformatics framework including structural modeling, docking with multiple Toll-like receptors (TLR2, TLR4, and TLR9), molecular dynamics (MD) simulations, binding free energy calculations, and immune response simulations, thereby providing a broader *in silico* characterization of vaccine–innate immune interactions.

Immunoinformatics-driven vaccine design provides an applied and cost-effective framework for prioritizing tuberculosis vaccine candidates before experimental testing. This study aims to design and evaluate an *in silico* multi-epitope tuberculosis vaccine candidate by integrating selected epitopes derived from Ag85B, ESAT-6, and HspX. To this end, comprehensive immunoinformatics analyses were performed, including predictions of antigenicity, immunogenicity, allergenicity, and toxicity, along with three-dimensional structural modeling, molecular docking, molecular dynamics simulations, and *in silico* immune response profiling.

MATERIALS AND METHODS

Retrieval of the antigen sequences

Amino acid sequences of Ag85B (UniProt ID: P9WQP1), ESAT-6 (UniProt ID: P9WNK7), and HspX (UniProt ID: P9WMK1) were retrieved from the UniProt database in FASTA format for subsequent computational analyses.

Prediction of CTL, HTL, and B-cell epitopes

CTL epitopes were predicted using NetMHCpan v4.1 (Reynisson, Alvarez, Paul, Peters, & Nielsen, 2020) with a binding threshold of 0.5, analyzing peptides of 9-11 amino acids. Binding affinity was assessed based on NetMHCpan scores, where lower values indicate stronger predicted binding. HTL epitopes were predicted using the IEDB MHC Class II (MHC-II) binding prediction tool (Vita et al., 2024) with a threshold value of 0.5, evaluating all alleles from HLA-DR, HLA-DP, and HLA-DQ loci. Linear B-cell epitopes were identified using multiple tools including ABCPred (Saha & Raghava, 2006), BcePred (Saha & Raghava, 2004), BepiPred-2.0 (Jespersen, Peters,

Nielsen, & Marcatili, 2017), and ElliPro (Ponomarenko et al., 2008) with default parameters recommended by each server.

Antigenicity, allergenicity, and toxicity evaluation

Antigenicity of selected proteins and epitopes was evaluated using VaxiJen v2.0 and VaxiJen v3.0 (Dimitrov, Zaharieva, & Doytchinova, 2020; Doneva & Dimitrov, 2024) with a threshold value of 0.4. Short linear B-cell epitopes were evaluated using VaxiJen v2.0 due to length limitations of VaxiJen v3.0. Additionally, allergenicity was predicted using AllerTOP v2.1 (Dimitrov, Bangov, Flower, & Doytchinova, 2014) and AlgPred 2.0 (Sharma et al., 2021) with default settings. Toxicity screening was performed using ToxinPred2 (Sharma, Naorem, Jain, & Raghava, 2022) with a threshold of 0.6. Only epitopes consistently predicted to be antigenic, non-allergenic, and non-toxic across all platforms were retained for vaccine construction.

Physicochemical property analysis

The physicochemical characteristics of the designed multi-epitope construct were analyzed using the ExPASy ProtParam server (Gasteiger et al., 2005). Parameters including molecular weight, theoretical isoelectric point (pI), instability index, aliphatic index, and grand average of hydropathicity (GRAVY) were computed to obtain physicochemical descriptors relevant to protein stability and solubility. The estimated half-life in various host systems (mammalian reticulocytes, yeast, and *E. coli*) was also determined.

Population coverage analysis

Population coverage for the selected CTL and HTL epitopes was calculated using the IEDB Population Coverage tool, based on their corresponding HLA class I and class II alleles. The analysis was performed using default parameters and evaluated the global population dataset provided by the tool.

Prediction of cytokine-inducing potential

The cytokine-inducing potential of CTL and HTL epitopes was evaluated using IFNepitope (Dhall Patiyal, & Raghava, 2024), IL2Pred (Mehta, Lathwal, Kumar, Kaur, & Raghava, 2025), IL4Pred (Dhanda, Gupta, Vir, & Raghava, 2013), IL6Pred (Dhall et al., 2020), and IL10Pred (Nagpal et al., 2017) servers with default thresholds. Epitopes predicted to induce interferon-γ (IFN-γ) and interleukin-2 (IL-2) responses were prioritized for inclusion in the final vaccine construct.

Epitope selection strategy

To ensure a transparent and systematic selection process, predicted epitopes were subjected to a multi-step filtering and prioritization strategy. Initially, CTL epitopes were predicted using NetMHCpan v4.1, HTL epitopes using the IEDB MHC-II binding prediction tool, and linear B-cell epitopes using the ABCPred, BcePred, BepiPred-2.0, and ElliPro tools. Predicted candidates were first screened based on their binding affinity and prediction scores. Subsequently, epitopes were filtered according to their immunological and safety profiles, and only those predicted to be antigenic (VaxiJen score > 0.4), non-allergenic (AllerTOP and AlgPred), and non-toxic (ToxinPred2) were retained.

For T-cell epitopes, predicted HLA-binding profiles and global population coverage were also evaluated to ensure broad immunological relevance. In addition, the cytokine-inducing potential of HTL epitopes was assessed using IFNepitope, IL2Pred, IL4Pred, IL6Pred, and IL10Pred, and epitopes predicted to stimulate key immune mediators such as IFN-γ and IL-2 were prioritized. Epitopes meeting all these criteria were subsequently selected for incorporation into the final multi-epitope vaccine construct. This stepwise screening pipeline ensured that only epitopes fulfilling predefined immunological, safety, and population coverage criteria were included in the final vaccine construct.

Design of the multi-epitope vaccine construct

The final vaccine construct was assembled by linking selected CTL, HTL, and B-cell epitopes using AAY, GPGPG, and KK linkers. AAY linkers were placed be-

tween CTL epitopes, GPGPG between HTL epitopes, KK between HTL and B-cell epitopes, and GGGGS between B-cell epitopes. Two adjuvants, Hp91 (DPNAPKRPPSAFFLFCSE) and RS09 (APPHALS), were incorporated at the N-terminus and linked via AAY spacers.

Codon optimization and *in silico* cloning

Codon optimization of the Vaccine Sequence (VS) for expression in human cells was performed using the VectorBuilder Codon Optimization Tool. The optimization strategy aligned codon usage with host-specific preferences while preserving the original amino acid sequence and maintaining appropriate GC content. The codon adaptation index (CAI) and GC content of the optimized sequence were recorded to assess expression efficiency. The optimized VS was subsequently cloned *in silico* into the pUC19 cloning vector at the Eco53kI restriction site. The vector was linearized using the Eco53kI restriction enzyme, and assembly of the recombinant construct was visualized and confirmed using SnapGene software.

Structural predictions and validation

The secondary structural composition of the designed vaccine construct was predicted using PSIPRED (Buchan, Moffat, Lau, Kandathil, & Jones, 2024). Three-dimensional structural modeling was performed using AlphaFold2 (Jumper et al., 2021), and the top-ranked model was refined using GalaxyRefine (Heo, Park, & Seok, 2013).

Model validation was carried out using ProSA-web for Z-score analysis (Wiederstein & Sippl, 2007), Verify3D for sequence–structure compatibility assessment, ERRAT for non-bonded interaction evaluation, and Ramachandran plot analysis for backbone torsion angle assessment. In addition, overall model quality was assessed using MolProbity, which evaluates steric clashes, rotamer outliers, and backbone geometry to generate a composite structure-validation score. Ramachandran plot analysis was performed using PROCHECK to evaluate the stereochemical quality of the models by examining the distribution of backbone dihedral angles (φ and ψ) and identifying residues in favored, additionally allowed, and disallowed regions.

Molecular docking with human toll-like receptors

The final 3D structure of the designed multi-epitope vaccine construct was docked with Toll-like receptor 2 (TLR2; PDB ID: 6NIG), Toll-like receptor 4 (TLR4; PDB ID: 3FXI), and Toll-like receptor 9 (TLR9; UniProt ID: Q9NR96). Because a complete experimental structure of TLR9 is not available, the full-length AlphaFold-predicted TLR9 model was used. Before docking, the TLR9 model was subjected to molecular dynamics simulation to reduce structural flexibility. Docking simulations were performed using the ClusPro 2.0 web server (Kozakov et al., 2017). Top-ranked complexes were selected according to ClusPro's scoring scheme. Interaction analysis of the docked complexes was conducted using PDBsum (Laskowski, Jabłońska, Pravda, Svobodová Vařeková, & Thornton, 2018), and the final complexes were visualized in PyMOL.

Molecular dynamics simulations of vaccine-TLR complexes

MD simulations were performed for each of the three vaccine-TLR complexes (VS–TLR2, VS–TLR4, and VS–TLR9) using GROMACS with the AMBER99SB force field. Each complex was solvated in a periodic water box and neutralized with 0.15 M concentration of sodium (Na^+) and chloride (Cl^-) ions. Energy minimization of the neutralized system was conducted using the steepest descent algorithm. Equilibration was carried out under NVT and NPT ensembles, after which 100 ns production MD simulations were performed at 300 K and 1 bar. Trajectory analyses included Root-mean-square deviation (RMSD), root-mean-square fluctuation (RMSF), radius of gyration (Rg), hydrogen bond counts, and solvent-accessible surface area (SASA).

Binding free-energy calculation

Binding free energies of the vaccine–TLR2, TLR4, and TLR9 complexes were estimated using the gmx_MMPBSA v1.6.3 tool based on the molecular dynam-

ics trajectories (Valdés-Tresanco, Valdés-Tresanco, Valiente, & Moreno, 2021). MM/GBSA calculations were performed using 1,000 frames extracted from the 0–100 ns interval, with the complex, receptor, and ligand components analyzed separately according to the MMPBSA protocol (Valdés-Tresanco et al., 2021). MM/GBSA calculations were carried out using the GB-Neck2 implicit solvent model (igb = 8).

In silico immune simulation

In silico immune response profiling was performed using the C-ImmSim server. The simulation followed a two-dose immunization schedule administered at four-week intervals (time steps 1 and 84). The simulation output included B-cell and T-cell population profiles, antibody isotypes (IgM, IgG1, IgG2), cytokine concentrations, and memory cell responses.

Data and code availability

All data generated or analyzed during this study are included in this published article and its Supplementary Materials. All computational tools used are publicly available. No custom code was generated.

Use of generative artificial intelligence

Generative artificial intelligence tools were used solely for language editing and refinement of the manuscript. No AI tools were used for data generation, analysis, interpretation, or figure creation.

RESULTS

Selection of antigenic proteins and epitope identification

The amino acid sequences of the selected *M. tuberculosis* antigens Ag85B, ESAT-6, and HspX used for immunoinformatics analyses are summarized in Table 1.

Table 1. Amino acid sequences of selected *Mycobacterium tuberculosis* antigens used for immunoinformatics analyses

Protein name	Protein sequence
Ag85B	MTDVSRKIRAWGRRLMIGTAAAVVLPGLVGLAGGAATAGAFSRPGLPVEYLQVPSPSMGRDIKVQFQSGGN NSPAVYLLGLRAQDDYNGWDINTPAFEWYYQSGLSIVMPVGGQSSFYSDWYSPACGKAGCQTYKWETFLTS ELPQWLSANRAVKPTGSAAIGLSMAGSSAMILAAYHPQQFIYAGSLSALLDPSQGMGPSLIGLAMGDAGGYK AANMWGPSSDPAWERNDPTQQIPKLVANNTRLWVYCGNGTPNELGGANIPAEFLKNFVRSSNLKFQDAY-NAAGGHNAVFNFPPNGTHSWEYWGAQLNAMKGDLQSSLGAG
ESAT-6	MTEQQWNFAGIEAAASAIQGNVTSIHSLLDEGKQSLTKLAAAWGGSGSEAYQGVQQKWDATATELNNALQ NLARTISEAGQAMASTEGNVTGMFA
HspX	MATTLPVQRHPRSLFPEFSELFAAFPSFAGLRPTFDTRLMRLEDEMKEGRYEVRAELPGVDPDKDVDIMVRD GQLTIKAERTEQKDFDGRSEFAYGSFVRTVSLPVGADEDDIKATYDKGILTVSVAVSEGKPTEKHIQIRSTN

A total of 886, 185, and 550 cytotoxic T lymphocyte (CTL) epitopes were initially predicted for Ag85B, ESAT-6, and HspX, respectively. Following filtering based on antigenicity, non-allergenicity, and non-toxicity criteria, 21 CTL epitopes were retained for Ag85B, 11 for ESAT-6, and 7 for HspX.

Helper T lymphocyte (HTL) epitope prediction across HLA-DP, HLA-DQ, and HLA-DR alleles yielded 171, 113, and 230 candidate epitopes, respectively. After applying stringent antigenicity, allergenicity, and toxicity filters, five HTL epitopes were retained for Ag85B and two for ESAT-6, whereas no HTL epitopes from HspX met the predefined selection criteria.

Global population coverage analysis identified a final set of epitopes comprising one Ag85B-derived MHC-I epitope, one HspX-derived MHC-I epitope, three Ag85B-derived MHC-II epitopes, and one ESAT-6-derived MHC-II epitope, which were incorporated into the final vaccine construct (Table 2.).

For B-cell epitope analysis, 423, 96, and 41 linear epitopes were predicted for Ag85B, ESAT-6, and HspX, respectively. Of these, 19 epitopes from Ag85B, three from ESAT-6, and three from HspX satisfied the selection thresholds and were retained for subsequent analyses (Table 2.).

Table 2. Selected MHC-I, MHC-II, and B-cell epitopes of Ag85B, ESAT-6, and HspX proteins following *in silico* screening

	Peptide	Antigenicity		Toxicity	Allergenicity		Population Coverage
		VaxiJen v2.0	VaxiJen v3.0	Toxinpred2	AllerTOP	AllergenFP	IEDB
Ag85B MHC-I	YLQVPSPSM	Probable antigen	Probable Immunogen with a probability of 100%.	Non-Toxin	Probable Non-Allergen	Non-Allergen	100.00%
HspX MHC-I	SFAGLRPTF	Probable antigen	Probable Non-Immunogen with a probability of 66%.	Non-Toxin	Probable Allergen	Non-Allergen	99.93%
Ag85B MHC-II	SWEYWGAQLNAMK	Probable antigen	Probable Immunogen with a probability of 66%.	Non-Toxin	Probable Non-Allergen	Non-Allergen	89.99%
	EYWGAQLNAMKG	Probable antigen	Probable Immunogen with a probability of 66%.	Non-Toxin	Probable Non-Allergen	Non-Allergen	85.66%
	SWEYWGAQLNAMKG	Probable antigen	Probable Non-Immunogen with a probability of 66%.	Non-Toxin	Probable Non-Allergen	Non-Allergen	99.95%
ESAT-6 MHC-II	MTEQQWNFAGIEAAASA	Probable antigen	Probable Immunogen with a probability of 100%.	Non-Toxin	Probable Allergen	Non-Allergen	88.07%
Ag85B B-cells	AAAVLPGLVGLAGGAATAGAFSRPGLPVEYLQVPSPSMGRDIKVQ	Probable antigen		Non-Toxin	Non-Allergen		-
	GDAGGYKAADMWGPSSDPAWERNDPTQQI	Probable antigen		Non-Toxin	Non-Allergen		-
	GLSIVMP	Probable antigen		Non-Toxin	Non-Allergen		-
	GLSMAGS	Probable antigen		Non-Toxin	Non-Allergen		-
	GLVGLAGAATAGAFSRPGLPVEYLQVPSPSMGRDIKVQFQSGGNN	Probable antigen		Non-Toxin	Non-Allergen		-
	GLVGLAGAATAGAFSRPGLPVEYLQVPSPSMGRDIKVQFQSGGNNSPA	Probable antigen		Non-Toxin	Non-Allergen		-
	GLVGLAGAATAGAFSRPGLPVEYLQVPSPSMGRDIKVQFQSGGNNSPAVYLLDG	Probable antigen		Non-Toxin	Non-Allergen		-
	GLVGLAGAATAGAFSRPGLPVEYLQVPSPSMGRDIKVQFQSGGNNSPAVYLLDGLRAQDDYNG	Probable antigen		Non-Toxin	Non-Allergen		-
	LVGLAGAATAGAFSRPGLPVEYLQVPSPSMGRDIKVQFQSGGNNSPAVYLLDGL	Probable antigen		Non-Toxin	Non-Allergen		-

Ag85B B-cells	VGLAGAATAGAFSRPGLPVEYLQVPSPSMGR-DIKVQFQSGGNNSP	Probable antigen	Non-Toxin	Non-Allergen	-
	GSSAMIL	Probable antigen	Non-Toxin	Non-Allergen	-
	IGLSMAGSSAMILAAY	Probable antigen	Non-Toxin	Non-Allergen	-
	LQVPSPSMGRDIKVQF	Probable antigen	Non-Toxin	Non-Allergen	-
	LSIVMPV	Probable antigen	Non-Toxin	Non-Allergen	-
	LSMAGSS	Probable antigen	Non-Toxin	Non-Allergen	-
	MILAAYH	Probable antigen	Non-Toxin	Non-Allergen	-
	MKGDLQS	Probable antigen	Non-Toxin	Non-Allergen	-
	PSPSMGR	Probable antigen	Non-Toxin	Non-Allergen	-
	SGLSIVM	Probable antigen	Non-Toxin	Non-Allergen	-
ESAT-6 B-cells	ARTISEAGQAMASTEG	Probable antigen	Non-Toxin	Non-Allergen	-
	MASTEGN	Probable antigen	Non-Toxin	Non-Allergen	-
	NVTSIHS	Probable antigen	Non-Toxin	Non-Allergen	-
HspX B-cells	IQIRSTN	Probable antigen	Non-Toxin	Non-Allergen	-
	KHIQIRS	Probable antigen	Non-Toxin	Non-Allergen	-
	MRLEDEMKEGRYEVRAELPG	Probable antigen	Non-Toxin	Non-Allergen	-

Cytokine-inducing potential of selected HTL epitopes

The cytokine-inducing potential of the selected HTL epitopes was evaluated to assess their immunostimulatory capacity. All six retained HTL epitopes were predicted to have the potential to induce interferon-γ (IFN-γ), interleukin-2 (IL-2), interleukin-4 (IL-4), and interleukin-6 (IL-6). Among these, one epitope derived from ESAT-6 (MTEQQWNFAGIEAAASA) was additionally predicted to induce interleukin-10 (IL-10) (Table 3.).

Table 3. Cytokine-inducing potential of selected HTL epitopes

	Peptide	IFN-γ	IL-2	IL-4	IL-6	IL-10
Ag85B_MHC-I	YLQVPSPSM	inducer	inducer	inducer	inducer	non-inducer
HspX_MHC-I	SFAGLRPTF	inducer	inducer	inducer	inducer	non-inducer
Ag85B_MHC-II	SWEYWGAQLNAMK	inducer	inducer	inducer	inducer	non-inducer
	EYWGAQLNAMKG	inducer	inducer	inducer	inducer	non-inducer
	SWEYWGAQLNAMKG	inducer	inducer	inducer	inducer	non-inducer
ESAT-6_MHC-II	MTEQQWNFAGIEAAASA	inducer	inducer	inducer	inducer	inducer

Multi-epitope vaccine construct design

A single multi-epitope vaccine construct, termed Vaccine Sequence (VS), was designed by integrating the selected T-cell (CTL and HTL) and B-cell epitopes derived from Ag85B, ESAT-6, and HspX. The epitopes were assembled using flexible AAY, KK, and GPGPG linkers to maintain structural separation. To enhance immunogenic potential, the adjuvants Hp91 (DPNAPKRPPSAFFLFCSE) and RS09 (APPHALS) were incorporated at the N-terminus of the construct via an AAY linker. The final vaccine construct consisted of 263 amino acids. A schematic representation of the construct is shown in Figure 1, and the complete sequence is provided in Supplementary Table 1.

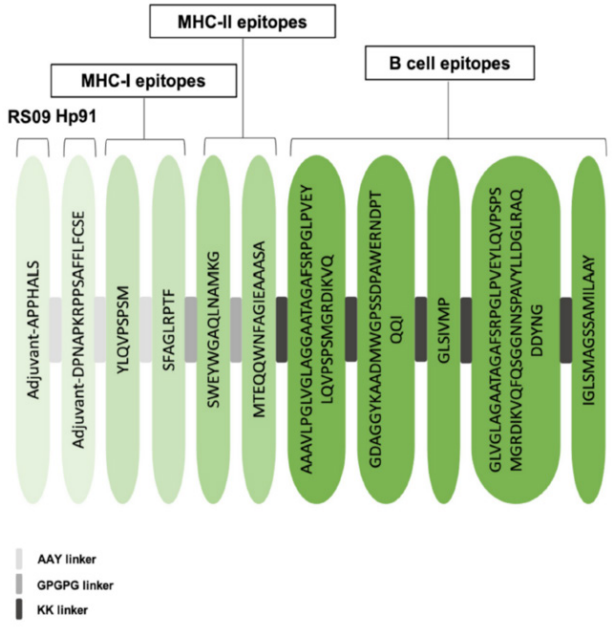

Figure 1. Schematic representation of the designed multi-epitope vaccine construct showing the arrangement of adjuvants, epitopes, and linkers

Immunological and safety assessment of the multi-epitope vaccine construct

The immunological and safety profiles of the VS were evaluated in terms of antigenicity, toxicity, and allergenicity.

Antigenicity analysis using VaxiJen v2.0 (score: 0.7231) and VaxiJen v3.0 predicted VS to be antigenic/immunogenic. According to ToxinPred2 predictions, the construct was predicted to be non-toxic. Allergenicity assessment using AllerTOP, AlgPred, and AllergenPro consistently predicted VS to be non-allergenic (Table 4.).

Table 4. Evaluation of antigenicity, toxicity. and allergenicity of VS

Antigenicity		**Toxicity**	**Allergenicity**		
VaxiJen v2.0	**VaxiJen v3.0**	**ToxinPred v2.0**	**AllergenPro**	**AllerTOP**	**AlgPred**
Antigen (0.7231)	Immunogen	Non-toxic	Antigen (0.8438)	Non-allergen	Non-allergen

Codon optimization and *in silico* cloning

The fused epitope sequence was successfully optimized for human expression, yielding a codon adaptation index (CAI) of 0.93 and a GC content of 54.10%, which may indicate a potential for efficient expression in mammalian systems. The optimized sequence was correctly inserted into the pUC19 cloning vector at the Eco53kI site. Analysis in SnapGene confirmed the proper orientation and integrity of the insert within the vector, demonstrating the successful *in silico* construction of the recombinant plasmid (Figure 2.).

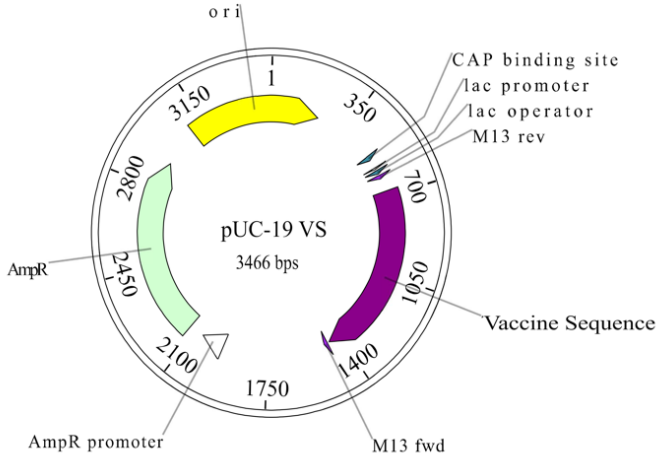

Figure 2. *In silico* visualization of the recombinant pUC19 cloning vector illustrating the insertion site and orientation of the codon-optimized VS sequence, generated using SnapGene software

Secondary structure analysis

The secondary structure analysis of the vaccine sequence revealed a predominance of α-helices, mainly distributed in the N-terminal and central regions, interspersed with coil segments that contribute to structural flexibility. Several β-strands were predicted primarily in the C-terminal region (Figure 3.).

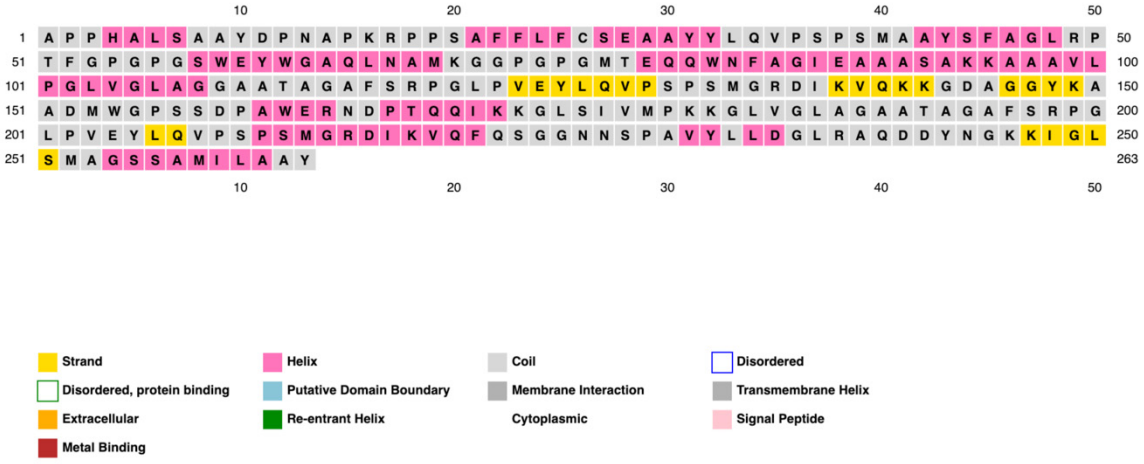

Figure 3. Two-dimensional (2D) structural representation of the designed multi-epitope VS. α-helix residues are shown in pink, β-strand residues in yellow, and coil regions in grey

Physicochemical profiling and stability analysis

The designed VS consists of 263 amino acids with a molecular weight of 27,195.01 Da and a theoretical isoelectric point (pI) of 9.30, indicating a basic protein. The predicted half-life was 4.4 h in mammalian reticulocytes, >20 h in yeast, and >10 h in *E. coli*. The instability index was calculated as 49.19, classifying the protein as unstable, while the aliphatic index was 68.86, suggesting moderate thermostability. The GRAVY value of −0.167 indicates an overall hydrophilic nature of the construct.

Structural refinement and validation of the vaccine model

The three-dimensional structure of the VS was refined using the GalaxyRefine server. Among the generated refinement models, the final structure was selected based on overall structural quality metrics provided by the server. The selected model exhibited a GDT-HA score of 0.8859 and an RMSD of 0.633.

Structural validation yielded a MolProbity score of 1.217, with a clash score of 4.4 and 0.5% poor rotamers. Ramachandran plot analysis showed that 98.1% of residues were located in favored regions. The ERRAT quality factor for the refined model was 80.69. VERIFY3D analysis indicated that 59.7% of residues met the 3D–1D compatibility criteria. ProSA-web analysis resulted in a Z-score of −4.69 (Figure 4.).

Molecular docking analysis with human TLRs

Docking analysis of the designed multi-epitope vaccine construct with human TLR2, TLR4, and TLR9 yielded weighted docking scores of −1230.3 for the TLR2–vaccine complex, −1482.1 for the TLR4–vaccine complex, and −2033.7 kcal/mol for the TLR9–vaccine complex.

Comparative evaluation of the docking scores showed that the TLR9–vaccine complex had the lowest (most negative) docking score, followed by the TLR4–vaccine and TLR2–vaccine complexes. Interface inspection suggested the presence of hydrogen bonds, electrostatic interactions, and hydrophobic contacts at the receptor–vaccine interfaces. The interacting residues were predominantly located within the adjuvant-containing region of the vaccine construct and the extracellular domains of the respective TLRs (Figure 5.).

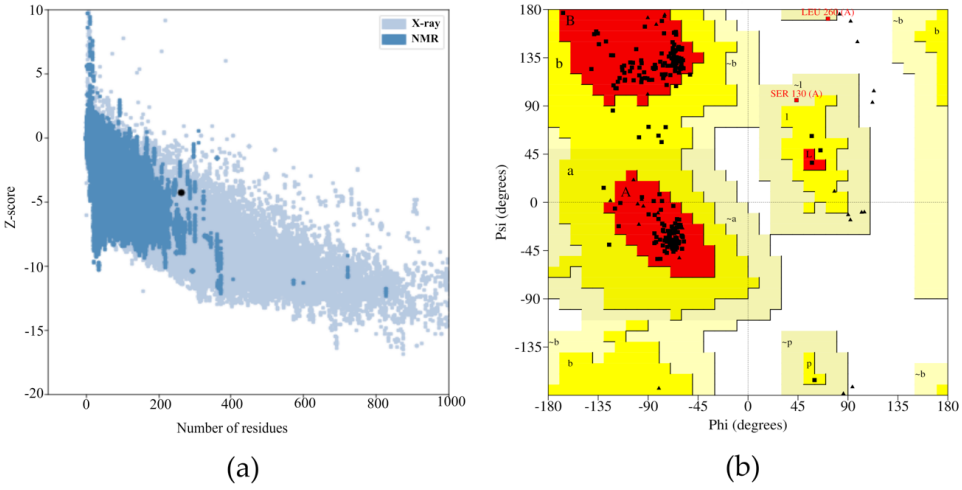

Figure 4. Structural validation analyses of the VS model showing (a) ProSA-web Z-score plot and (b) Ramachandran plot

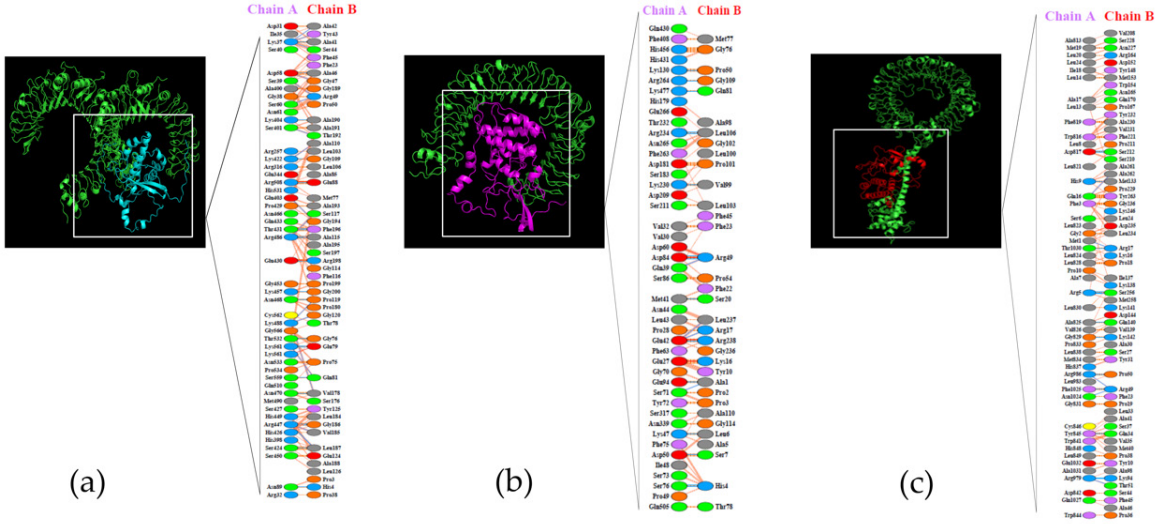

Figure 5. Docked complexes of the designed multi-epitope vaccine construct with human TLR2 (a), TLR4 (b), and TLR9 (c)

Normal mode analysis of vaccine–TLR complexes

Normal mode analysis (NMA) was performed to investigate the dynamic behavior of the vaccine–TLR complexes. The deformability profiles (Figure 6a; Supplementary Figures 1a and 2a) indicated overall limited atomic displacements for all complexes, with localized flexible regions. Among them, the TLR2–vaccine complex showed the lowest deformability peaks (maximum ~0.4), followed by the TLR4–vaccine complex (~0.6), whereas the TLR9–vaccine complex exhibited higher peaks near the binding interface, reaching ~0.9.

The B-factor profiles (Figure 6b; Supplementary Figures 1b and 2b) were consistent with the deformability analysis, showing lower atomic fluctuations for the TLR2 and TLR4 complexes, while the TLR9 complex displayed localized regions of increased mobility, particularly toward the terminal segments.

Eigenvalue analysis (Figure 6c; Supplementary Figures 1c and 2c) revealed differences in resistance to

deformation among the complexes. The lowest eigenvalue was observed for the TLR9–vaccine complex (3.36×10^{-6}), followed by the TLR2–vaccine (1.75×10^{-5}) and TLR4–vaccine (2.92×10^{-5}) complexes.

Elastic network models (Figure 6d; Supplementary Figures 1d and 2d) further demonstrated variations in network density, with the TLR2–vaccine complex exhibiting a denser connectivity pattern compared to the more diffuse network observed for the TLR9–vaccine complex.

Covariance matrix analysis (Figure 6e; Supplementary Figures 1e and 2e) showed distinct patterns of correlated atomic motions. The TLR9–vaccine complex displayed dominant positively correlated motions, whereas the TLR2–vaccine complex showed a higher proportion of anti-correlated motions.

Finally, the elastic network model representations (Figure 6f; Supplementary Figures 1f and 2f) illustrated the distribution of inter-residue connections within each complex, further highlighting the compact network organization of the TLR2–vaccine complex in contrast to the more dispersed connectivity observed for the TLR9–vaccine complex, with the TLR4–vaccine complex showing intermediate features.

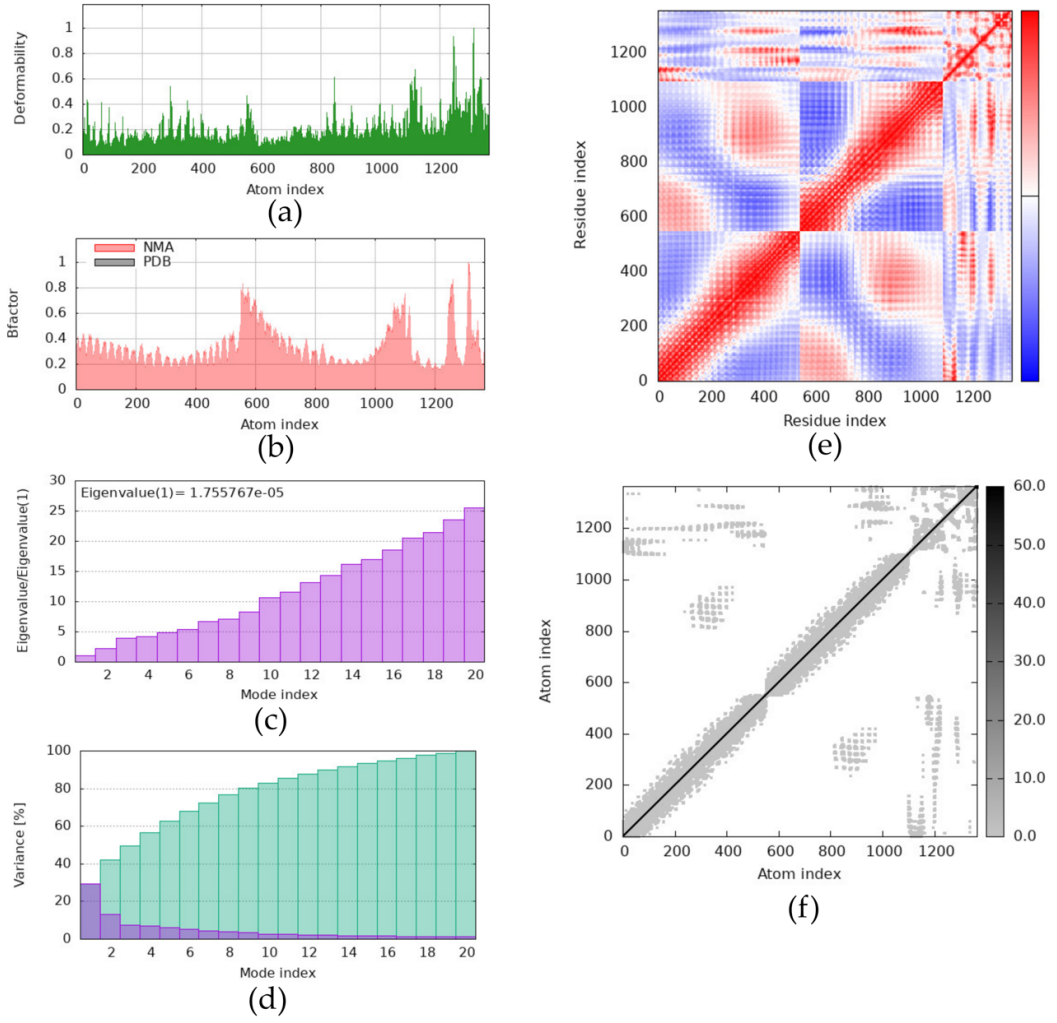

Figure 6. Normal mode analysis of the VS–TLR2 complex. (a) Deformability profile. (b) B-factor distribution. (c) Eigenvalue distribution. (d) Mode-wise variance contribution. (e) Covariance matrix of atomic fluctuations. (f) Elastic network model illustrating interatomic connectivity

Structural validation, TLR fusion stability, and predicted immune response potential

ProSA-web analysis was applied to evaluate the overall model quality of the docking-derived vaccine–TLR complexes. The calculated Z-scores were −6.59 for the TLR2–vaccine complex, −7.84 for the TLR4–vaccine complex, and −9.81 for the TLR9–vaccine complex. All Z-scores fell within the range commonly reported for experimentally determined protein structures of comparable size.

The residue-wise energy profiles generated by ProSA-web showed that the majority of residues in all three complexes were located within negative energy regions, suggesting thermodynamically stable conformations. Differences in the depth and distribution of negative energy regions were observed among the complexes, with the TLR4– and TLR9–vaccine complexes displaying broader regions of negative energy compared to the TLR2–vaccine complex, as shown in Supplementary Figure 3.

Molecular dynamics simulation of vaccine–TLR complexes

RMSD analysis of the vaccine sequence in complex with TLR2, TLR4, and TLR9 over a 100 ns simulation period showed initial fluctuations during the equilibration phase (~0–10 ns), followed by stable trajectories for the remainder of the simulations (Figure 7a.). The TLR4–vaccine complex displayed the highest RMSD values, reaching a plateau of approximately 0.8 nm after ~30 ns. The TLR2–vaccine complex stabilized earlier with an average RMSD of ~0.7 nm, while the TLR9–vaccine complex showed the lowest RMSD values, plateauing around ~0.65 nm.

Residue-level flexibility was evaluated using RMSF analysis (Figure 7b.). The TLR9–vaccine complex exhibited higher RMSF values at several regions, with peaks exceeding 0.6 nm, particularly within residues 75–120. In contrast, the TLR2–vaccine complex showed lower RMSF values across most residues, whereas the TLR4–vaccine complex displayed intermediate fluctuations, with localized peaks observed around residues 150–160. All three complexes shared regions of low fluctuation, notably between residues 50–65.

Radius of gyration (Rg) profiles remained stable throughout the simulation period for all complexes, suggesting preservation of overall structural integrity (Figure 7c.). The TLR4–vaccine complex exhibited the lowest average Rg values (~3.0 nm), followed by the TLR2–vaccine complex (~4.0 nm), while the TLR9–vaccine complex showed higher Rg values (~4.7–5.0 nm).

Solvent-accessible surface area (SASA) analysis showed stabilization of surface exposure over time for all complexes (Figure 7d.). The TLR4–vaccine complex displayed lower SASA values (~370 nm^2) compared to the TLR2– and TLR9–vaccine complexes, which exhibited higher SASA values (~600 nm^2), particularly during the early stages of the simulation. SASA values for all systems converged after approximately 20 ns.

Intermolecular hydrogen bond analysis revealed sustained hydrogen bonding throughout the simulation period for all complexes (Figure 7e.). The TLR4–vaccine complex maintained the highest number of hydrogen bonds, ranging from approximately 15 to 25, followed by the TLR2–vaccine complex (approximately 10–22) and the TLR9–vaccine complex (approximately 10–20).

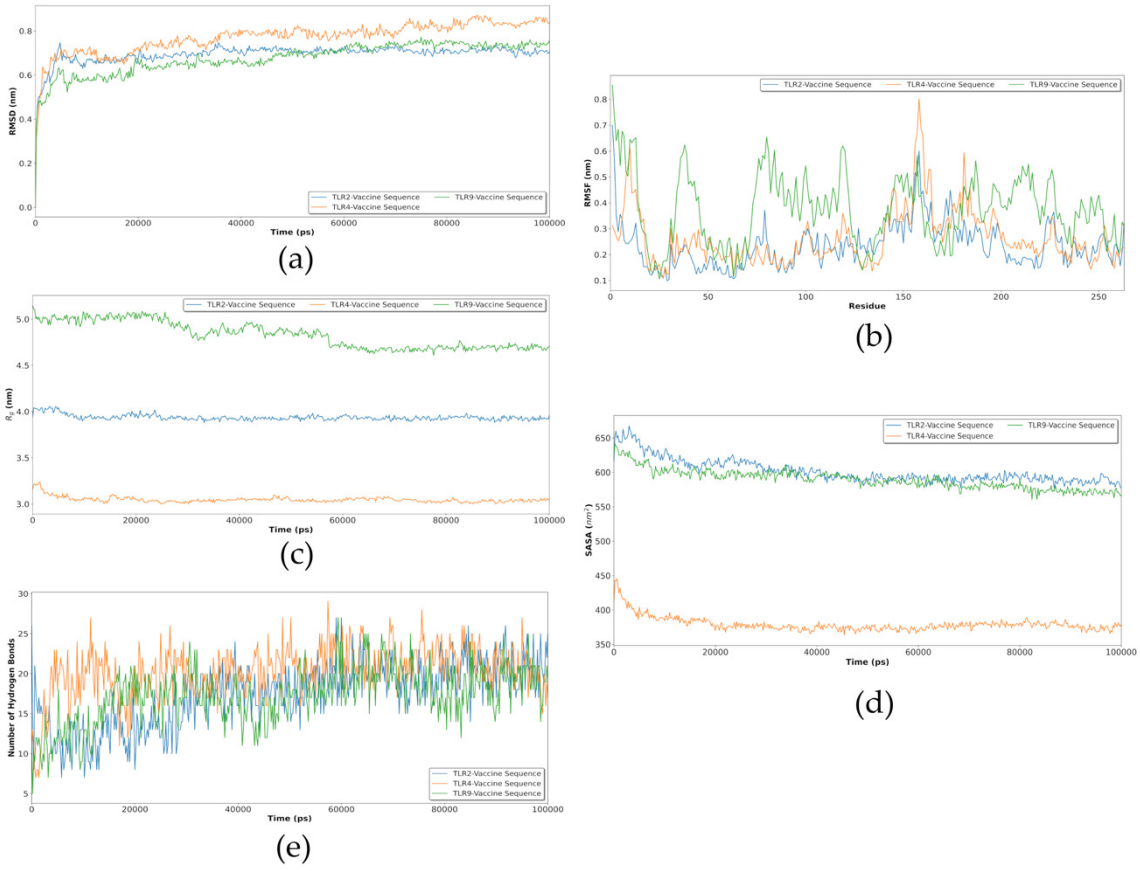

Figure 7. Molecular dynamics simulation analyses of the vaccine sequence in complex with human TLR2, TLR4, and TLR9. (a) Root mean square deviation (RMSD) profiles of the vaccine–TLR complexes. (b) Root mean square fluctuation (RMSF) profiles of the vaccine sequence residues. (c) Radius of gyration (Rg) profiles. (d) Solvent-accessible surface area (SASA) profiles. (e) Intermolecular hydrogen bond (H-bond) profiles between the vaccine sequence and TLR2, TLR4, and TLR9 during the simulation period

Binding free energy calculation

The binding free energies of the vaccine sequence in complex with TLR2, TLR4, and TLR9 were estimated using MM/GBSA analysis (Table 5). The calculated total binding free energy (ΔTOTAL) values were −249.46 kJ/mol for the TLR2–vaccine complex, −240.26 kJ/mol for the TLR4–vaccine complex, and −392.27 kJ/mol for the TLR9–vaccine complex.

Among the three complexes, the TLR9–vaccine complex exhibited the most negative ΔTOTAL value. Van der Waals interactions (ΔVDWAALS) contributed substantially to the total binding free energy in all complexes, with the largest contribution observed for the TLR9 complex (−353.98 kJ/mol). Electrostatic energy (ΔEEL) contributions varied among the complexes, with more pronounced electrostatic contributions observed for the TLR2 and TLR4 complexes.

The gas-phase energy terms (ΔGGAS) were favorable for all three systems, whereas the solvation free energy components (ΔGSOLV) partially offset these contributions. The TLR4–vaccine complex showed the highest polar solvation energy (ΔEGB = 179.34 kJ/mol), while the TLR9–vaccine complex exhibited comparatively lower solvation energy contributions. The resulting balance of gas-phase and solvation energies yielded distinct total binding free energy profiles for each complex (Table 5.).

Table 5. Binding free energy analysis of vaccine sequence-TLR complexes

Energy component	TLR2	TLR4	TLR9
ΔVDWAALS (kJ/mol)	-228.78	-211.70	-353.98
ΔEEL (kJ/mol)	-89.18	-176.07	-3.11
ΔEGB (kJ/mol)	99.96	179.34	13.60
ΔGGAS (kJ/mol)	-317.96	-387.77	-357.09
ΔGSOLV (kJ/mol)	68.50	147.51	-35.18
ΔTOTAL (kJ/mol)	-249.46	-240.26	-392.27

In silico immune simulation

Immune simulation results for the VS construct suggested dynamic changes in both humoral and cellular immune components following sequential antigen exposures. After the two injections, the simulation indicated increases in antigen-presenting cells, naïve $CD4^+$ and $CD8^+$ T-cells, and B-cell populations, accompanied by elevated cytokine levels (Figure 8.).

Analysis of cytokine levels suggested distinct temporal expression patterns. IL-2 levels were predicted to increase following both injections, while IFN-γ and TNF-α levels were predicted to be elevated during the post-injection phases. In later stages of the simulation, increased levels of IL-4 and IL-10 were predicted, along with a moderate predicted induction of TGF-β.

Epitope mapping analysis predicted multiple peptides capable of interacting with MHC class I and II molecules. Notably, the peptides YLQVPSPSM, APPHALSAA, and LSMAGSSAM were predicted to be associated with potential $CD8^+$ and $CD4^+$ T-cell responses.

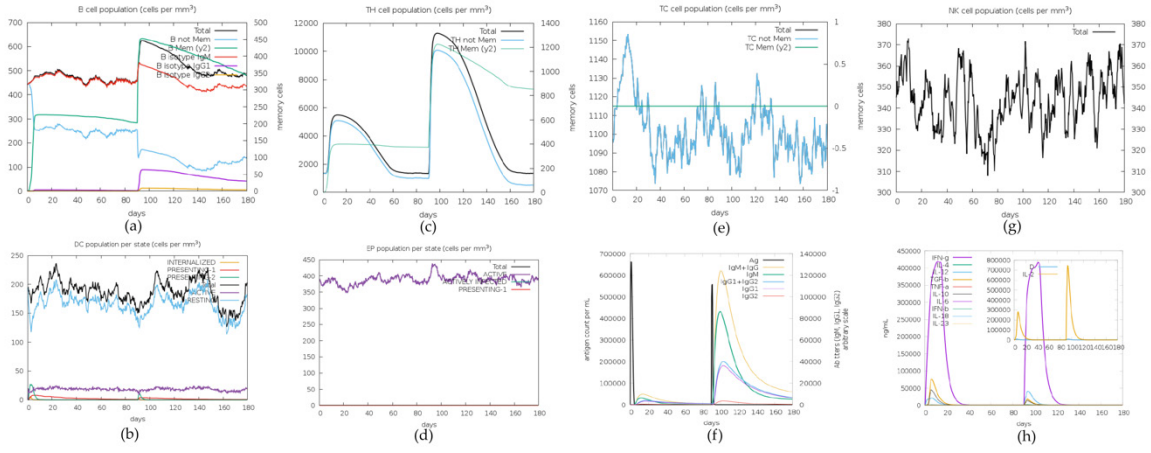

Figure 8. Immune simulation of the VS showing dynamic humoral and cellular responses following two simulated injections. (a) B-cell population dynamics and isotype switching. (b) Dendritic cell (DC) populations in different functional states. (c) Helper T-cell (TH) population profile. (d) Epithelial cell (EP) population states. (e) Cytotoxic T-cell (TC) population dynamics. (f) Antigen levels and antibody titers (IgM, IgG1, IgG2). (g) Natural killer (NK) cell population dynamics. (h) Cytokine concentration profiles, including IFN-γ, IL-2, IL-4, IL-10, and TNF-α

DISCUSSION

Tuberculosis (TB) remains a major global public health challenge, with millions of new cases and substantial mortality reported annually despite ongoing control efforts (Suvvari, 2025; WHO, 2024). Although the Bacillus Calmette–Guérin (BCG) vaccine is widely used, its protective efficacy is limited, particularly in adolescents and adults who account for the ma-

jority of TB cases (Ari et al., 2024). These limitations underscore the need for alternative vaccine strategies capable of inducing robust and long-lasting immune responses. In this context, immunoinformatics-based approaches have emerged as valuable tools for rational vaccine design, enabling systematic epitope selection and construct optimization (Akurut et al., 2025; Barazani et al., 2025; Faysal et al., 2024; Singh et al., 2025; Yun et al., 2024). Consistent with this trend, multiple next-generation TB vaccine candidates are currently advancing through clinical development pipelines (An et al., 2025; WHO, 2024).

In the present study, a multi-epitope vaccine construct (VS) was designed by integrating cytotoxic T lymphocyte (CTL), helper T lymphocyte (HTL), and B-cell epitopes derived from three well-characterized *M. tuberculosis* antigens Ag85B, ESAT-6, and HspX, which are associated with distinct stages of infection (An et al., 2025; Gurmessa et al., 2025; Hidalgo-Gajardo, Mangui, Villavicencio, Toledo, & Camacho, 2025; Srivastava Dey, & Mukhopadhyay, 2023). This stage-spanning antigen selection strategy is intended to promote broader immune coverage by targeting both early secretory and latent-phase antigens. The simultaneous inclusion of CTL, HTL, and B-cell epitopes may support a balanced immune stimulation profile, potentially enabling the activation of both cellular and humoral immune responses (Akurut et al., 2025; Barazani et al., 2025; Urdahl, 2014). In addition, the broad population coverage predicted for the selected epitopes may indicate potential applicability across diverse human populations.

Comprehensive immunoinformatics analyses suggested that the VS construct may exhibit favorable antigenic properties while remaining non-toxic and non-allergenic, suggesting potential relevance for vaccine development (Bemani, Amirghofran, & Mohammadi, 2020; Rani et al., 2025). The incorporation of the Hp91 and RS09 adjuvant sequences may contribute to enhanced innate immune activation and promote downstream adaptive immune responses, as previously reported for peptide-based vaccine constructs (Bemani et al., 2020; Rani et al., 2025). Moreover, the use of flexible AAY, KK, and GPGPG linkers may help preserve epitope integrity and reduce the risk of junctional immunogenicity, thereby potentially facilitating effective epitope presentation.

Physicochemical characterization and structural validation collectively provided insights into the expressibility and stability of the VS construct. The construct's molecular size, basic isoelectric point, hydrophilic character, and codon optimization parameters may indicate suitability for recombinant expression and favorable solubility. Structural validation using ProSA-web and Ramachandran plot analysis supported the stereochemical accuracy and energetic plausibility of the predicted three-dimensional model, supporting its suitability for downstream interaction and dynamic analyses (Mirzaie, Yuan, Ni, & Wu, 2025; Nugraha et al., 2024; Ullah, Ullah, Fatima, & Lei, 2025). The physicochemical analysis predicted an instability index of 49.19, which exceeds the commonly accepted stability threshold of 40 and therefore suggests potential instability according to sequence-based estimation methods. However, the instability index represents a theoretical prediction derived from the amino acid composition and does not necessarily reflect the actual stability of recombinant proteins under experimental conditions (Gamage, Gunaratne, Periyannan, & Russell, 2019). A predicted instability in this range may nonetheless warrant closer attention during recombinant expression, as it could translate into a higher susceptibility to intracellular proteolytic degradation or reduced yield, depending on the host expression system used (Guruprasad, Reddy, & Pandit, 1990). In artificial fusion proteins such as multi-epitope vaccine constructs, linker regions and concatenated epitope sequences may influence the structural organization of the protein (Chen Zaro, & Shen, 2013; Shamriz, Ofoghi, & Moazami, 2016). Variations in linker length and composition have been reported to influence protein folding and structural stability. Therefore, sequence-based stability estimations

should be interpreted with caution in such engineered constructs. Previous immunoinformatics-based vaccine design studies have similarly reported constructs with instability index values above the conventional threshold while still demonstrating favorable physicochemical properties and suitability for recombinant expression when evaluated together with additional parameters such as aliphatic index and GRAVY score (Ghafouri, Ahangari Cohan, Noorbakhsh, Samimi, & Haghpanah, 2020). Notably, in a related computational vaccine design study, despite an elevated instability index value, the designed multi-epitope construct exhibited appropriate physicochemical characteristics and subsequently induced strong humoral and cellular immune responses in animal experiments. These findings suggest that the instability index alone may not be sufficient to determine the functional stability or immunogenic potential of engineered vaccine constructs. In the present study, the moderate aliphatic index and the negative GRAVY value indicating hydrophilicity further support the possibility that the designed construct may remain compatible with recombinant expression and solubility. Nevertheless, experimental expression, purification, and stability analyses will be required to confirm the biochemical stability of the vaccine construct.

In addition to the validation approaches mentioned above, structural validation of computationally predicted protein models is typically performed using multiple complementary evaluation tools rather than relying on a single metric. Methods such as Ramachandran plot analysis, ERRAT, ProSA, MolProbity, and VERIFY3D evaluate different aspects of model quality, including stereochemical geometry, non-bonded interactions, energy profiles, and sequence–structure compatibility (Mamun et al., 2025; Naveed et al., 2026; Saadh et al., 2024; Sharma Yadav, & Cherian, 2025; Shetty et al., 2024). Therefore, structural reliability is generally interpreted based on the combined outcomes of these validation approaches rather than a single score alone.

In the present study, the VERIFY3D compatibility score was relatively modest (59.7%), falling below the conventional 80% threshold. This finding does not necessarily indicate an invalid model; rather, it reflects a known limitation of VERIFY3D when applied to engineered fusion proteins: the designed construct represents a concatenated epitope assembly connected by linker regions rather than a naturally occurring globular protein, and such fusion constructs often contain flexible and non-standard structural regions that may not fully conform to the statistical potentials derived from native protein structures (Kumar & Kim, 2024). Similar observations have been reported in several previous immunoinformatics-based multi-epitope vaccine design studies, in which models with VERIFY3D compatibility values below the conventional 80% threshold were still considered structurally acceptable when evaluated alongside complementary validation metrics such as Ramachandran plots, ProSA, and ERRAT analyses (Forouharmehr, Banan, Mousavi, & Jaydari, 2022; Hashemzadeh, Ghorbanzadeh, Lashgarian, Kheirandish, & Dariushnejad, 2020). Therefore, for engineered multi-epitope constructs, structural quality is more appropriately interpreted based on multiple validation criteria rather than a single VERIFY3D score.

Interactions between the VS construct and innate immune receptors provided insight into its predicted immunological potential. Molecular docking analyses suggested stable binding interactions with TLR2, TLR4, and TLR9, with compact and well-aligned interfaces indicative of efficient molecular recognition (Huang et al., 2025). Engagement of TLR2, which plays a key role in early recognition of *M. tuberculosis* components, may contribute to rapid cytokine signaling during initial immune activation (Park et al., 2020). Similarly, interaction with TLR4, known to promote sustained NF-κB and IRF signaling, may support TH1-biased cellular immune responses. The interaction with TLR9 displayed a more flexible yet energetically stable binding mode, which may be advantageous for endosomal sensing mechanisms and

memory-associated immune responses (Gurmessa et al., 2025; Hidalgo-Gajardo et al., 2025; Srivastava et al., 2023). Together, these findings suggest that simultaneous engagement of multiple TLRs may contribute to coordinated innate activation and downstream adaptive immune responses.

Normal mode analysis (NMA) and molecular dynamics (MD) simulations further characterized the dynamic behavior of the vaccine–TLR complexes. Receptor-dependent differences in flexibility and resistance to deformation were observed, with the TLR2–vaccine complex exhibiting lower deformability and a denser elastic network, whereas the TLR9–vaccine complex showed higher deformability peaks, lower eigenvalues, and more pronounced correlated motions, indicating greater intrinsic flexibility. The TLR4–vaccine complex displayed intermediate dynamic features between these systems. Stable RMSD and RMSF profiles throughout the MD simulations suggested persistent interactions across the complexes, supporting their overall structural stability. In addition, sustained hydrogen bond networks and reduced solvent-accessible surface area in specific complexes were consistent with the formation of relatively stable interaction interfaces.

Energetic evaluation using MM/GBSA analysis revealed receptor-specific binding profiles, with the TLR9–vaccine complex exhibiting a comparatively more favorable total binding free energy. Van der Waals interactions constituted the dominant energetic contribution, underscoring the importance of hydrophobic contacts in stabilizing vaccine–TLR interactions. When integrated with docking and MD results, these findings collectively suggest a coherent computational assessment of interaction stability.

Finally, *in silico* immune simulation indicated that the VS construct may be capable of eliciting coordinated cellular and humoral immune responses. Elevated interferon-γ and interleukin-2 levels were consistent with a potential TH1-oriented immune profile, while moderate induction of interleukin-4 and interleukin-10 reflected activation of humoral and regulatory pathways. The predicted expansion of memory B and T-cell populations following booster exposure may suggest the potential establishment of durable immunological memory and sustained immune protection.

CONCLUSION

This study suggests that a rationally designed, stage-spanning multi-epitope vaccine construct incorporating experimentally validated *M. tuberculosis* antigens exhibits favorable predicted immunological, structural, and dynamic interaction profiles *in silico*. By integrating antigens associated with both early and latent stages of infection and systematically evaluating their interactions with multiple innate immune receptors, this work provides a more comprehensive computational assessment than many prior single-target vaccine designs. While these findings support the potential of the designed vaccine construct as a promising candidate for tuberculosis vaccine development, they remain entirely computational and should therefore be interpreted with appropriate caution. Comprehensive experimental validation, including *in vitro* immunogenicity and expression studies followed by *in vivo* efficacy and safety evaluations, will be essential to confirm the predicted immunological properties, structural stability, and protective potential of the proposed vaccine. Overall, this study provides a robust computational framework that may facilitate the rational design and prioritization of next-generation tuberculosis vaccine candidates for subsequent experimental investigation.

LIMITATIONS

The primary limitation of the present study is its exclusively computational nature, which cannot fully capture the complexity of antigen processing, presentation, immune regulation, and host-pathogen interactions *in vivo* and therefore necessitates comprehensive experimental validation to verify the computational predictions under biological conditions. Additionally, uncertainties associated with epitope

prediction accuracy, structural modeling of artificial sequences, and receptor docking based on predicted receptor structures may influence the robustness of the computational predictions. Nevertheless, such *in silico* approaches represent a critical first step in modern vaccine research, enabling the systematic screening and prioritization of antigenic candidates before more resource-intensive *in vitro* and *in vivo* studies. The convergence of results obtained from multiple independent bioinformatics platforms and complementary computational tools strengthens the overall reliability and internal consistency of the predictions while helping to reduce methodological bias. Nevertheless, as with all computational vaccine design studies, experimental validation remains essential to confirm the predicted immunological properties, structural stability, and protective potential of the proposed vaccine construct under biological conditions. Such validation will be critical for translating these computational findings into practical vaccine development.

FUTURE DIRECTIONS

Future studies should focus on the experimental validation of the multi-epitope DNA vaccine developed in this work. As a first step, expression of the vaccine construct should be evaluated in appropriate mammalian cell systems, while recombinant expression in *E. coli* may be used for protein production and biochemical characterization. These studies should assess expression efficiency, structural stability, solubility, and production feasibility. Subsequently, the antigen presentation capacity and TLR interactions should be examined *in vitro* to experimentally confirm the immunogenic potential predicted *in silico*. The immunogenicity, protective efficacy, and safety profile of the vaccine candidate should then be evaluated *in vivo*, particularly in mice previously immunized with BCG, to verify the computational predictions and determine its complementary protective efficacy alongside the existing BCG vaccine. Finally, testing the construct containing epitopes specific to human MHC alleles in MHC-humanized mouse models will be essential to validate its interaction potential with the human immune system. Only through this sequential experimental validation process can the computational findings presented in this study be confirmed and the translational potential of the proposed vaccine construct be reliably established before clinical development.

AUTHOR CONTRIBUTION STATEMENT

Methodology, Software, Validation, and Formal Analysis: (SK), (SA), (ECB); Investigation, Resources, and Data Curation: (SK), (SA), (ECB); Writing – Review & Editing: (SK), (SA), (ECB); Visualization: (SK); Project Administration: (SK), (SA).

CONFLICT OF INTEREST

The authors declare that there is no conflict of interest.

REFERENCES

Akurut, E., Gavamukulya, Y., Mulindwa, J., Isiagi, M., Galiwango, R., Bbuye, M., … Mboowa, G. (2025). Design of a multi-epitope vaccine against drug-resistant Mycobacterium tuberculosis and Mycobacterium bovis using reverse vaccinology. *Scientific Reports, 15*, 27298. doi:10.1038/s41598-025-11768-3

Ali, S., Ali, U., Safi, K., Naz, F., Jan, M. I., Iqbal, Z., … Bari, A. (2024). In silico homology modeling of dengue virus non-structural 4B (NS4B) protein and its molecular docking studies using triterpenoids. *BMC Infectious Diseases, 24*, 688. doi:10.1186/s12879-024-09578-5

An, Y., Ni, R., Zhuang, L., Yang, L., Ye, Z., Li, L., … Gong, W. (2025). Tuberculosis vaccines and therapeutic drug: challenges and future directions. *Molecular Biomedicine, 6*, 4. doi:10.1186/s43556-024-00243-6

Anes, E., Pires, D., Mandal, M., & Azevedo-Pereira, J. M. (2023). ESAT-6 a major virulence factor of Mycobacterium tuberculosis. *Biomolecules, 13*, 968. doi:10.3390/biom13060968

Ari, M. M., Beig, M., Sholeh, M., & Khoshmirsafa, M. (2024). The BCG vaccine, advantages, and disadvantages of introducing new generation vaccines against Mycobacterium tuberculosis. *Clinical and Experimental Vaccine Research, 13*(3), 184–201. doi:10.7774/cevr.2024.13.3.184

Bahadori, Z., Shafaghi, M., Madanchi, H., Ranjbar, M. M., Shabani, A. A., & Mousavi, S. F. (2022). In silico designing of a novel epitope-based candidate vaccine against Streptococcus pneumoniae with introduction of a new domain of PepO as adjuvant. *Journal of Translational Medicine, 20*, 389. doi:10.1186/s12967-022-03590-6

Barazani, O., Erdos, T., Chowdhury, R., Kaur, G., & Venketaraman, V. (2025). New advances in the development and design of Mycobacterium tuberculosis vaccines: Construction and validation of multi-epitope vaccines for tuberculosis prevention. *Biology, 14*, 417. doi:10.3390/biology14040417

Bemani, P., Amirghofran, Z., & Mohammadi, M. (2020). Designing a multi-epitope vaccine against blood-stage malaria by in silico approaches. *Journal of Molecular Graphics and Modelling, 99*, 107645. doi:10.1016/j.jmgm.2020.107645

Buchan, D. W. A., Moffat, L., Lau, A., Kandathil, S. M., & Jones, D. T. (2024). Deep learning for the PSIPRED protein analysis workbench. *Nucleic Acids Research, 52*(W1), W287–W293. doi:10.1093/nar/gkae328

Bulla, A. C. S., Sbano da Silva, A., Prado Sereno, B., Ribeiro Dias, M. F., & Leal da Silva, M. (2025). Computational methods in immunoinformatics: Epitope discovery and diagnostic applications. *ACS Omega, 10*, 44816–44839. doi:10.1021/acsomega.5c05538

Chen, X., Zaro, J., & Shen, W.-C. (2013). Fusion protein linkers: property, design and functionality. *Advanced Drug Delivery Reviews, 65*(10), 1357–1369. doi:10.1016/j.addr.2012.09.039

Deepthi, V., Sasikumar, A., Mohanakumar, K. P., & Rajamma, U. (2025). Computationally designed multi-epitope vaccine construct targeting the SARS-CoV-2 spike protein elicits robust immune responses in silico. *Scientific Reports, 15*, 9562. doi:10.1038/s41598-025-92956-z

Dhall, A., Patiyal, S., Sharma, N., Usmani, S. S., & Raghava, G. P. S. (2020). Computer-aided prediction and design of IL-6 inducing peptides: IL-6 plays a crucial role in COVID-19. *Briefings in Bioinformatics, 22*(2), 936–945. doi:10.1093/bib/bbaa259

Dhall, A., Patiyal, S., & Raghava, G. P. S. (2024). A hybrid method for discovering interferon-gamma inducing peptides in human and mouse. *Scientific Reports, 14*, 26859. doi:10.1038/s41598-024-77957-8

Dhanda, S. K., Gupta, S., Vir, P., & Raghava, G. P. S. (2013). Prediction of IL4 inducing peptides. *Clinical and Developmental Immunology, 2013*, 263952. doi:10.1155/2013/263952

Dimitrov, I., Bangov, I., Flower, D. R., & Doytchinova, I. (2014). AllerTOP v.2—A server for in silico prediction of allergens. *Journal of Molecular Modeling, 20*, 2278. doi:10.1007/s00894-014-2278-5

Dimitrov, I., Zaharieva, N., & Doytchinova, I. (2020). Bacterial immunogenicity prediction by machine learning methods. *Vaccines, 8*(4), 709. doi:10.3390/vaccines8040709

Doneva, N., & Dimitrov, I. (2024). Viral immunogenicity prediction by machine learning methods. *International Journal of Molecular Sciences, 25*, 2949. doi:10.3390/ijms25052949

Faysal, M. A., Tanni, F. Y., Rahman, M. M., Rahman, M. A., Chowdhury, M. S. R., Cho, H.-S., … Uddin, M. B. (2024). In silico driven multi-epitope subunit candidate vaccine against bovine tuberculosis. *Transboundary and Emerging Diseases, 2024*, 5534041. doi:10.1155/2024/5534041

Forouharmehr, A., Banan, A., Mousavi, S. M., & Jaydari, A. (2022). Development of a novel multi-epitope vaccine candidate against Streptococcus iniae infection in fish: An immunoinformatics study. *Archives of Razi Institute, 77*, 45–56. doi:10.22092/ARI.2021.353377.1601

Gamage, D. G., Gunaratne, A., Periyannan, G. R., & Russell, T. G. (2019). Applicability of instability index for in vitro protein stability prediction. *Protein and Peptide Letters, 26*(5), 339–347. doi:10.2174/0929866526666190228144219

Gasteiger, E., Hoogland, C., Gattiker, A., Duvaud, S., Wilkins, M. R., Appel, R. D., & Bairoch, A. (2005). Protein identification and analysis tools on the ExPASy server. In J. M. Walker (Ed.), *The proteomics protocols handbook* (pp. 571–607). Totowa, NJ: Humana Press. doi:10.1385/1-59259-890-0:571

Ghafouri, F., Ahangari Cohan, R., Noorbakhsh, F., Samimi, H., & Haghpanah, V. (2020). An in-silico approach to develop of a multi-epitope vaccine candidate against SARS-CoV-2 envelope (E) protein. *Research Square* [Preprint]. doi:10.21203/rs.3.rs-30374/v1

Gurmessa, S. K., Choi, H.-G., Back, Y. W., Jiang, Z., Pham, T. A., Choi, S., & Kim, H.-J. (2025). Novel fusion protein REA induces robust prime protection against tuberculosis in mice. *npj Vaccines, 10*, 20. doi:10.1038/s41541-025-01077-1

Guruprasad, K., Reddy, B. V. B., & Pandit, M. W. (1990). Correlation between stability of a protein and its dipeptide composition: A novel approach for predicting in vivo stability of a protein from its primary sequence. *Protein Engineering, 4*(2), 155–161. doi:10.1093/protein/4.2.155

Hashempour, A., Khodadad, N., Akbarinia, S., Ghasabi, F., Ghasemi, Y., Karbalaei Ali Nazar, M. M., & Falahi, S. (2024). Reverse vaccinology approaches to design a potent multiepitope vaccine against the HIV whole genome: Immunoinformatic, bioinformatics, and molecular dynamics approaches. *BMC Infectious Diseases, 24*, 873. doi:10.1186/s12879-024-09775-2

Hashemzadeh, P., Ghorbanzadeh, V., Lashgarian, H. E., Kheirandish, F., & Dariushnejad, H. (2020). Harnessing bioinformatic approaches to design a novel multi-epitope subunit vaccine against Leishmania infantum. *International Journal of Peptide Research and Therapeutics, 26*, 1417–1428. doi:10.1007/s10989-019-09949-6

Heo, L., Park, H., & Seok, C. (2013). GalaxyRefine: Protein structure refinement driven by side-chain repacking. *Nucleic Acids Research, 41*(W1), W384–W388. doi:10.1093/nar/gkt458

Hidalgo-Gajardo, A., Mangui, B., Villavicencio, C., Toledo, J. R., & Camacho, F. (2025). Targeting HspX of Mycobacterium tuberculosis: Advances in diagnostics, treatment, and vaccine development. *Tuberculosis, 155*, 102702. doi:10.1016/j.tube.2025.102702

Huang, Z., Deng, C., Peng, L., Shang, L., Jiang, J., Yu, W., … Wang, X. (2025). Self-assembling TLR2 agonists promote mucosal immune responses without pulmonary immunopathologic injuries. *npj Vaccines, 10*, 127. doi:10.1038/s41541-025-01185-y

Jespersen, M. C., Peters, B., Nielsen, M., & Marcatili, P. (2017). BepiPred-2.0: Improving sequence-based B-cell epitope prediction using conformational epitopes. *Nucleic Acids Research, 45*(W1), W24–W29. doi:10.1093/nar/gkx346

Jiang, F., Han, Y., Liu, Y., Xue, Y., Cheng, P., Xiao, L., & Gong, W. (2023). A comprehensive approach to developing a multi-epitope vaccine against Mycobacterium tuberculosis: From in silico design to in vitro immunization evaluation. *Frontiers in Immunology, 14*, 1280299. doi:10.3389/fimmu.2023.1280299

Jumper, J., Evans, R., Pritzel, A., Green, T., Figurnov, M., Ronneberger, O., … Hassabis, D. (2021). Highly accurate protein structure prediction with AlphaFold. *Nature, 596*, 583–589. doi:10.1038/s41586-021-03819-2

Kozakov, D., Hall, D. R., Xia, B., Porter, K. A., Padhorny, D., Yueh, C., … Vajda, S. (2017). The ClusPro web server for protein–protein docking. *Nature Protocols, 12*, 255–278. doi:10.1038/nprot.2016.169

Kumar, H., & Kim, P. (2024). Artificial intelligence in fusion protein three-dimensional structure prediction: Review and perspective. *Clinical and Translational Medicine, 14*, e1789. doi:10.1002/ctm2.1789

Laskowski, R. A., Jabłońska, J., Pravda, L., Svobodová Vařeková, R., & Thornton, J. M. (2018). PDBsum: Structural summaries of PDB entries. *Protein Science, 27*, 129–134. doi:10.1002/pro.3289

Lew, M. H., Norazmi, M. N., Nordin, F., & Tye, G. J. (2022). A novel peptide vaccination augments cytotoxic CD8+ T-cell responses against Mycobacterium tuberculosis HspX antigen. *Immunobiology, 227*, 152201. doi:10.1016/j.imbio.2022.152201

Lim, H. X., Masomian, M., Khalid, K., Kumar, A. U., MacAry, P. A., & Poh, C. L. (2022). Identification of B-cell epitopes for eliciting neutralizing antibodies against the SARS-CoV-2 spike protein through bioinformatics and monoclonal antibody targeting. *International Journal of Molecular Sciences, 23*(8), 4341. doi:10.3390/ijms23084341

Mamun, T. I., Ali, M. A., Hosen, M. N., Rahman, J., Islam, M. A., Akib, M. G., … Dawoud, T. M. (2025). Designing a multi-epitope vaccine candidate against human rhinovirus C utilizing immunoinformatics approach. *Frontiers in Immunology, 15*, 1364129. doi:10.3389/fimmu.2024.1364129

Mehta, N. K., Lathwal, A., Kumar, R., Kaur, D., & Raghava, G. P. S. (2025). In silico tool for predicting, designing and scanning IL-2 inducing peptides. *Scientific Reports, 15*, 25692. doi:10.1038/s41598-025-08388-2

Mirzaie, S., Yuan, K. D., Ni, H., & Wu, X. Y. (2025). Design of a novel multiepitope vaccine against glioblastoma by in silico approaches. *Scientific Reports, 15*, 24046. doi:10.1038/s41598-025-03672-7

Musunuri, S., Weidenbacher, P. A. B., & Kim, P. S. (2024). Bringing immunofocusing into focus. *npj Vaccines, 9*, 11. doi:10.1038/s41541-023-00792-x

Nagpal, G., Usmani, S. S., Dhanda, S. K., Kaur, H., Singh, S., Sharma, M., & Raghava, G. P. S. (2017). Computer-aided designing of immunosuppressive peptides based on IL-10 inducing potential. *Scientific Reports, 7*, 42851. doi:10.1038/srep42851

Naveed, M., Husnain, M., Aziz, T., Qadir, P., Asim, M., Majeed, M. N., … Tombozara, N. (2026). Immunoinformatics-based design and evaluation of a multi-epitope vaccine against Vibrio fluvialis. *Scientific Reports, 16*, 4100. doi:10.1038/s41598-026-35434-4

Nugraha, M. F., Changestu, D. A., Ramadhan, R., Salsabila, T., Nurizati, A., Pratiwi, S. E., & Ysrafil, Y. (2024). Novel prophylactic and therapeutic multi-epitope vaccine based on Ag85A, Ag85B, ESAT-6, and CFP-10 of Mycobacterium tuberculosis using an immunoinformatics approach. *Osong Public Health and Research Perspectives, 15*, 286–306. doi:10.24171/j.phrp.2024.0026

Park, J., Kim, H., Kwon, K. W., Choi, H.-H., Kang, S. M., Hong, J. J., & Shin, S. J. (2020). Toll-like receptor 4 signaling-mediated responses are critically engaged in optimal host protection against highly virulent Mycobacterium tuberculosis K infection. *Virulence, 11*(1), 430–445. doi:10.1080/21505594.2020.1766401

Ponomarenko, J., Bui, H.-H., Li, W., Fusseder, N., Bourne, P. E., Sette, A., & Peters, B. (2008). ElliPro: A new structure-based tool for the prediction of antibody epitopes. *BMC Bioinformatics, 9*, 514. doi:10.1186/1471-2105-9-514

Rani, S., Khatoon, M., Pyasi, S., Kunbhar, B. V., Patil, S. S., Barman, N. N., … Suresh, K. P. (2025). Comprehensive immunoinformatics approach for developing a multi-epitope subunit vaccine against lumpy skin disease. *Veterinary Vaccine, 4*, 100146. doi:10.1016/j.vetvac.2025.100146

Reynisson, B., Alvarez, B., Paul, S., Peters, B., & Nielsen, M. (2020). NetMHCpan-4.1 and NetMHCIIpan-4.0: Improved predictions of MHC antigen presentation by concurrent motif deconvolution and integration of MS MHC eluted ligand data. *Nucleic Acids Research, 48*(W1), W449–W454. doi:10.1093/nar/gkaa379

Saadh, M. J., Ahmed, H. H., Kareem, R. A., Baldaniya, L., Verma, L., Prasad, G. V. S., … Hamad, A. K. (2024). Design of a novel multi-epitope vaccine candidate against Yersinia pestis using advanced immunoinformatics approaches: An in silico study. *Biochemistry and Biophysics Reports, 40*, 101871. doi:10.1016/j.bbrep.2024.101871

Saha, S., & Raghava, G. P. S. (2004). BcePred: Prediction of continuous B-cell epitopes in antigenic sequences using physico-chemical properties. In G. Nicosia, V. Cutello, P. J. Bentley, & J. Timmis (Eds.), *Artificial immune systems* (pp. 197–204). Berlin, Germany: Springer. doi:10.1007/978-3-540-30220-9_16

Saha, S., & Raghava, G. P. S. (2006). Prediction of continuous B-cell epitopes in an antigen using recurrent neural network. *Proteins: Structure, Function, and Bioinformatics, 65*(1), 40–48. doi:10.1002/prot.21078

Shamriz, S., Ofoghi, H., & Moazami, N. (2016). Effect of linker length and residues on the structure and stability of a fusion protein with malaria vaccine application. *Computers in Biology and Medicine, 76*, 24–29. doi:10.1016/j.compbiomed.2016.06.015

Sharma, N., Naorem, L. D., Jain, S., & Raghava, G. P. S. (2022). ToxinPred2: An improved method for predicting toxicity of proteins. *Briefings in Bioinformatics, 23*(5), bbac174. doi:10.1093/bib/bbac174

Sharma, N., Patiyal, S., Dhall, A., Pande, A., Arora, C., & Raghava, G. P. S. (2021). AlgPred 2.0: An improved method for predicting allergenic proteins and mapping of IgE epitopes. *Briefings in Bioinformatics, 22*(4), bbaa294. doi:10.1093/bib/bbaa294

Sharma, S., Yadav, P. D., & Cherian, S. (2025). Comprehensive immunoinformatics and bioinformatics strategies for designing a multi-epitope-based vaccine targeting structural proteins of Nipah virus. *Frontiers in Immunology, 16*, 1535322. doi:10.3389/fimmu.2025.1535322

Shetty, S., Dash, S., Kumar, A., Vishwanath, S., Kini, S. G., & Brand, A. (2024). Immunoinformatics design of a multi-epitope vaccine for Chlamydia trachomatis major outer membrane proteins. *Scientific Reports, 14*, 29919. doi:10.1038/s41598-024-81736-w

Singh, S., Verma, P., Gaur, M., Bhati, L., Madan, R., Sharma, P. P., … Singh, M. (2025). In-silico development of a novel TLR2-mediating multi-epitope vaccine against Mycobacterium tuberculosis. *In Silico Pharmacology, 13*, 34. doi:10.1007/s40203-025-00322-8

Srivastava, S., Dey, S., & Mukhopadhyay, S. (2023). Vaccines against tuberculosis: Where are we now? *Vaccines, 11*(5), 1013. doi:10.3390/vaccines11051013

Stop TB Partnership. (2022). *The global plan to end TB 2023–2030*. Geneva, Switzerland: Author.

Suvvari, T. K. (2025). The persistent threat of tuberculosis—Why ending TB remains elusive? *Journal of Clinical Tuberculosis and Other Mycobacterial Diseases, 38*, 100510. doi:10.1016/j.jctube.2025.100510

Teibo, T. K. A., Andrade, R. L. de P., Rosa, R. J., de Abreu, P. D., Olayemi, O. A., Alves, Y. M., … Arcêncio, R. A. (2024). Barriers that interfere with access to tuberculosis diagnosis and treatment across countries globally: A systematic review. *ACS Infectious Diseases, 10*, 2600–2614. doi:10.1021/acsinfecdis.4c00466

Ullah, S., Ullah, H., Fatima, K., & Lei, T. (2025). In silico designed multi-epitope vaccine based on the conserved fragments in viral proteins for broad-spectrum protection against porcine reproductive and respiratory syndrome virus. *Veterinary Sciences, 12*(6), 577. doi:10.3390/vetsci12060577

United Nations General Assembly. (2018). *Political declaration of the High-Level Meeting of the General Assembly on the fight against tuberculosis* (A/RES/73/3). New York, NY: United Nations.

United Nations General Assembly. (2023). *Political declaration of the High-Level Meeting on the fight against tuberculosis* (A/RES/78/5). New York, NY: United Nations.

Urdahl, K. B. (2014). Understanding and overcoming the barriers to T cell-mediated immunity against tuberculosis. *Seminars in Immunology, 26*(6), 578–587. doi:10.1016/j.smim.2014.10.003

Valdés-Tresanco, M. S., Valdés-Tresanco, M. E., Valiente, P. A., & Moreno, E. (2021). gmx_MMPBSA: A new tool to perform end-state free energy calculations with GROMACS. *Journal of Chemical Theory and Computation, 17*(10), 6281–6291. doi:10.1021/acs.jctc.1c00645

Vita, R., Blazeska, N., Marrama, D., IEDB Curation Team Members, Duesing, S., Bennett, J., … Peters, B. (2024). The Immune Epitope Database (IEDB): 2024 update. *Nucleic Acids Research, 53*(D1), D436–D443. doi:10.1093/nar/gkae1092

Wiederstein, M., & Sippl, M. J. (2007). ProSA-web: Interactive web service for the recognition of errors in three-dimensional structures of proteins. *Nucleic Acids Research, 35*(Suppl. 2), W407–W410. doi:10.1093/nar/gkm290

World Health Organization. (2020). *Global tuberculosis report 2020*. Geneva, Switzerland: Author.

World Health Organization. (2022). *Global tuberculosis report 2022*. Geneva, Switzerland: Author.

World Health Organization. (2023a). *Global tuberculosis report 2023*. Geneva, Switzerland: Author.

World Health Organization. (2023b). *The second United Nations high-level meeting on the fight against tuberculosis*. Retrieved from https://www.who.int/news-room/events/detail/2023/09/22/default-calendar/the-second-united-nations-high-level-meeting-on-the-fight-to-end-tuberculosis

World Health Organization. (2024). *Global tuberculosis report 2024*. Geneva, Switzerland: Author.

World Health Organization. (2025). *WHO consolidated operational handbook on tuberculosis: Module 4: Treatment and care*. Geneva, Switzerland: Author.

Yun, J.-S., Kim, A. R., Kim, S. M., Shin, E., Ha, S.-J., Kim, D., & Jeong, H.-S. (2024). In silico analysis for the development of multi-epitope vaccines against Mycobacterium tuberculosis. *Frontiers in Immunology, 15*, 1474346. doi:10.3389/fimmu.2024.1474346

Zubair, S., Parvaiz, F., Abualait, T., Al-Regaiey, K., Anwar, T., Zafar, M., … Bashir, S. (2025). Computational design of multi-epitope vaccine against hepatitis C virus infection using immunoinformatics techniques. *PLOS ONE, 20*(1), e0317520. doi:10.1371/journal.pone.0317520